

Development of a Direct Correlation of Bead Geometry, Grain Size and HAZ Width with the GMAW Process Parameters on Bead-on-plate Welds of Mild Steel

Deb Kumar Adak · Manidipto Mukherjee ·
Tapan Kumar Pal

Received: 3 September 2014 / Accepted: 22 January 2015 / Published online: 4 March 2015
© The Indian Institute of Metals - IIM 2015

Abstract In this study, an experimental work was conducted to correlate the effect of gas metal arc welding (GMAW) process parameters such as wire feed speed, voltage, and contact tip to work piece distance along with interactive variables on bead-on-plate weld characteristics using multiple linear regression analysis and ANOVA (analysis of variance). The different responses such as convexity index, depth of penetration, reinforcement area, deposition rate, width of heat affected zone (HAZ), weld metal grain size and HAZ grain size were studied. The aim of the present investigation is to develop multiple linear regression equations to predict different responses (outputs) as a function of multiple input variables for ‘bead-on-plate’ type GMAW process. Multiple linear regression equations were first developed for weld bead geometry as a function of several individual and interactive variables. Then an effort was made to effectively predict the grain structure of the weldments as a function of multiple variables. Predicted responses are very close and sometime superimposed on the actual responses which clearly indicate the adequacy of the regression equations.

Keywords Gas metal arc welding · Bead-on-plate · Multiple linear regression analysis · Weld characteristics

1 Introduction

The relationship between arc welding parameters, weld bead geometry and grain structure is complex since a number of factors are involved. Yet there is a need to have this information for procedure development and for understanding the mechanism of weld bead formation along with the grain structure in automated welding equipment such as with the gas metal arc welding (GMAW) process [1]. GMAW is a highly complex, multi-variable system, in which the variables affecting weld quality are not explicitly known. Thus, developing a model for making predictions of weld bead geometry has turned out to be crucial. Several researchers have attempted to investigate the effects of various process variables on the weld bead geometry. Such work published prior to 1978 has been summarized by Shinoda and Doherty [2]. Subsequent to the above publication, Chandel et al. [3] were successful in predicting the effect of current, electrode polarity, electrode diameter and electrode extension on the melting rate and bead geometry in submerged arc welding and found that both electrode extension and polarity were important variables. Jou [4] developed a 3-D FEM model for a single pass gas tungsten arc (GTA) welding to predict both the transient thermal histories as well as weld pool geometries. Results of the FEM simulations were found to match with those of real experiments. Gunaraj and Murugan [5] developed the mathematical models for the bead-on-plate and bead-on-joint processes for submerged arc welding of pipes. Area of the heat-affected zone was well represented by both the models and followed the same trend. The authors [6] further obtained the models for submerged arc welding process using a five-level factorial technique and response surface methodology. In a continuation of this work [7], mathematical models were derived (together with sensitivity

D. K. Adak (✉)
Mechanical Engineering Department, College of Engineering
and Management, Kolaghat, India
e-mail: debkumaradak1968@gmail.com

M. Mukherjee · T. K. Pal
Metallurgical and Material Engineering Department, Jadavpur
University, Kolkata, India

analysis), for optimization (minimization) of total bead volume (keeping other bead parameters as constraints) and determination of optimum process parameters, to ensure better weld quality, increased productivity and minimum welding cost. Kim et al. [8, 9] carried out a sensitivity analysis for a robotic gas metal arc welding (GMAW) process, to determine the effect of measurement errors on the uncertainty in estimated parameters. They used non-linear multiple regression analysis for modeling the process and identified the respective effects of process parameters on the weld bead-geometric parameters. In another work, Kim et al. [10] determined both linear as well as non-linear multiple regression equations, to relate the welding process parameters with the weld bead-geometric parameters, in robotic CO₂ arc welding. The developed response equations were able to predict the weld bead geometry with sufficient accuracy from the process parameters. Lee and Rhee [11] conducted an investigation of the gas metal arc welding process (i.e., butt welding with groove gap), where both forward (i.e., from process parameters to response) as well as backward (i.e., from response to process parameters) relations were determined through multiple regression analysis and the mean deviations in prediction were seen to lie within 9.5 and 6.5 %, respectively. Recently, Ganjigatti et al. [12] have attempted to establish input–output relationships in MIG welding process through regression analyses carried out both globally (i.e., one set of response equations for the entire range of the variables) as well as cluster-wise. It was found that the cluster-wise regression analysis is found to perform slightly better than the global approach in predicting weld bead-geometric parameters. Gunaraj et al. [13] also developed regression models to predict the bead and heat affected zone characteristics using central composite rotatable factorial design matrix and the adequacy of the models was tested by the analysis-of-variance technique (ANOVA). Their study revealed that the heat input and wire feed rate have a positive effect, but welding speed has a negative effect on all bead and HAZ characteristics. They also concluded that the width of grain growth and grain refinement zones increased and weld interface decreased with an increase in arc voltage and the width of HAZ is greatest when wire-feed rate and welding speed are at their minimum limits. Among the several characteristic responses, the weld deposit area or the reinforcement area, deposition rate, width of HAZ, weld metal grain size and HAZ grain size are also the significant responses apart from general bead geometry [14]. These responses are significant because they not only affect the bead size, base metal dilution, and number of passes required to fill a joint, but also provide an insight on the metallurgical features.

So far it is observed that all the previous research works has tried only to develop a model by which the relationship

between process parameters and weld bead geometry can be predicted. But there is no predictive model available in the literature which can predict grain size of the weldments from the process parameters. Therefore, in this investigation, an attempt is made to study the influence of basic welding parameters (i.e. wire feed speed, contact tip to workpiece distance and voltages) on the weld bead geometry (such as convexity index, depth of penetration, reinforcement area), deposition rate, width of HAZ, weld metal grain size and HAZ grain size. The aim of the present investigation is to develop multiple linear regression equations to predict different responses (outputs) as a function of multiple input variables for ‘bead-on-plate’ type GMAW process. Multiple linear regression equations were first developed for weld bead geometry as a function of several individual and interactive variables. Then an effort was made to effectively predict the grain structure of the weldments as a function of multiple variables.

2 Experimental Procedure

In the present work, a mild steel plate having 0.15 % carbon of size 150 × 150 × 9 mm was used as base metal to prepare bead on plates using ER80S-G, a commercially available uncoated filler wire of diameter 1.2 mm. Details of bead on plate preparation for the GMAW process are shown in Fig. 1. The chemical composition of the base material and filler wire are given in Table 1.

Among the several factors, wire feed speed (WFS), welding voltage (V), contact tip to workpiece distance (CTWD) are considered as the chosen inputs or process parameters. In this work, sufficient numbers of trial experiments have been carried out to find the parameter ranges in which effective welding takes place without failure (such as power failure due to short circuit and discontinuous arching). Two levels are considered for each of the three input process parameters (refer to Table 2), and thus, $2^3 = 8$ combinations of input process parameters are to be considered for the full-factorial design of experiment (DOE).

The experiments were conducted using a Kemppi, Finland make water Cooled Universal MIG/MAG machine (Model: Evolution Pro4200) using DC electrode positive (DCEP). The Combinations of input process parameters along with other associated parameters in un-coded form are given in Table 3. Heat input was calculated using the standard formula (i.e. VI/WS) as given in Table 3, where VI is the power input and WS is the welding speed, which gives heat input per unit length. However, heat input is a function of welding speed though they are separate because without changing the heat input welding speed can be varied and vice versa. Bead on plate welding was

Fig. 1 Dimension of base plates used for preparing bead on plates

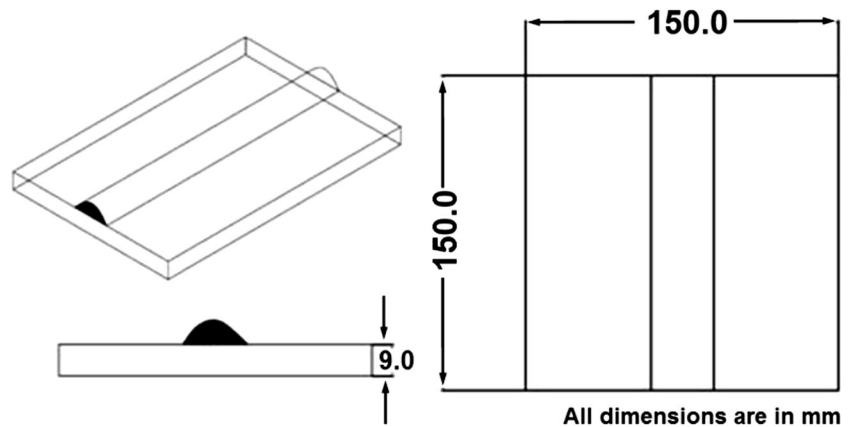


Table 1 Chemical compositions (in wt%) of base metal & filler wire

Type	C	Mn	Si	S	P	Cr	Ni	Mo	V	W	Cu	Al	B
Base metal	0.147	0.79	0.02	0.011	0.014	0.036	0.019	0.001	0.0013	0.038	0.0078	0.057	0.0008
Filler wire	0.099	1.13	0.64	0.011	0.01	0.052	0.84	0.006	0.001	0.049	0.405	0.003	0.0008

Table 2 Experimental parameter setup with low level and high level significance

Level	Voltage (V)	WFS (m/min)	CTWD (mm)	Level significance
0	19.8	3.5	15	Low
1	24	5.5	25	High

Table 3 Design of experiment by 2³ factorial design and other process parameters

Sl. No	Voltage (V)	WFS (m/min)	CTWD (mm)	WS (mm/min)	Current (Amp)	HI (kJ/mm)
1.	19.8	3.5	15	250	137	0.586
2.	19.8	5.5	15		194	0.830
3.	24	3.5	15		133	0.689
4.	24	5.5	15		181	0.938
5.	19.8	3.5	25		121	0.517
6.	19.8	5.5	25		143	0.611
7.	24	3.5	25		119	0.616
8.	24	5.5	25		164	0.850

WFS wire feed speedm, CTWD contact tip to workpiece distance, S welding speed, HI heat input ($V \times I \times \eta \times 60/WS \times 1000$)

performed using the selected welding parameters. The welding operations were performed using 70 % Ar + 30 % CO₂ shielding gas mixture. A contact torch angle was maintained at 20° for all the weld deposits. A welding speed of 250 mm/min was also maintained during all the operation. All necessary care was taken to avoid distortion and the welding was made with applying proper clamping (i.e. pneumatic grip and C-clamp) devices.

Once the welding is over, all welded plates were cut perpendicular to the welding direction using a power saw machine to measure the weld bead geometry along with the other features. A schematic diagram of the bead geometry is shown in Fig. 2. Two specimens (cross sectional specimen centering the weld axis) were cut from each plate 5 cm away from the start and the end point. The cut surfaces were flattened through belt grinding and were polished successively with #120, #180, #220, #320, #400, #600, #800, #1000, #1200 silicon carbide abrasive papers. The specimens were further polished in a polishing wheel using diamond compound of 9, 6, 3, 1, 0.25 micron wet Selvyt cloth/micro cloth followed by final polishing with 0.05 micron slurry of Al₂O₃ (diluted by distilled water in 9:1

ratio) on a fine micro cloth. The specimens were then washed, cleaned with distilled water and ethanol and dried by a drier. After polishing, those samples were etched with Nital solution (2 % HNO₃). The macrographs and micrographs of all the specimens were taken in a Carl Zeiss Microscope. The bead geometry parameters such as bead width (W), bead height (H), bead penetration (P), bead toe angle (θ) and reinforcement area (A_R) and other features like width of HAZ and grain size were measured using AutoCAD 2010 software. Grain size of weld metal and HAZ were measured by linear intercept method. The average values of all the data (from the two cuts) were calculated for each experiment. The complete weld bead geometry parameters and other features of each welding condition are given in Table 4.

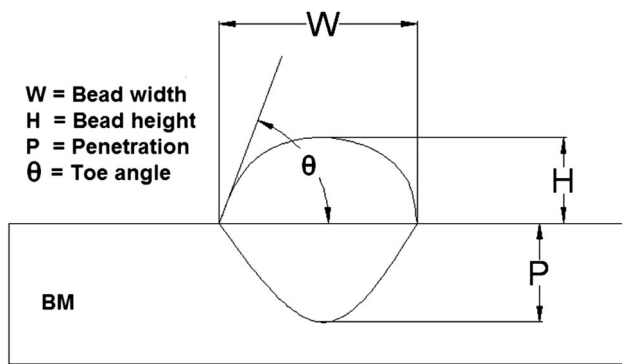


Fig. 2 A schematic diagram of weld bead geometry

Finally, multiple regression analysis was carried out on the data collected as per full-factorial design of experiments to predict different responses. In this study, the responses considered are like the following: convexity index (H/W), bead penetration (P), reinforcement area (A_R), deposition rate (D_R), width of HAZ (W_{HAZ}), HAZ grain size (d_{HAZ}) and weld metal grain size (d_{WM}). The adequacy of the models was then tested by the analysis-of-variance technique (ANOVA).

3 Results and Discussion

3.1 The Effect of Process Parameters on Bead Geometry

The macro views of the bead (bead appearance and bead geometry), welded with different WFS, CTWD and Voltage were captured and shown in Fig. 3. The values of bead geometry such as bead height (H), bead width (W) and depth of penetration (P) were measured from the macrographs using AutoCAD 2010 software and all the data are presented in Table 4. The convexity index or the reinforcement height to bead width ratio along with toe angles

are also provided in Table 4. The optimum level for a factor is the level that gives the desired quality characteristics in the experimental region. Rao et al. [15] argued that the desired quality characteristic for penetration is the bigger-the-better, and for convexity index, the desired quality characteristic is the-smaller-the-better.

By varying several process parameters and due to their combined effect different bead profiles can be achieved. Figure 4 shows several contour plots depicting the effect of process parameters on the bead geometry. In this study, contour plots are used due to the fact that it is able to depict the profile of higher and/or lower concentration of the objective functions in a precise manner, which is merely difficult to achieve in other diagrams. Significant increase in bead height, width and penetration were obtained with the increase in WFS at a particular arc voltage and CTWD (Fig. 4a–c). Higher WFS increases the current and thus increases the deposition rate (Table 4) which has two fold effects on the bead geometry. Higher current increases the downward fluid flow at molten weld pool and increase the primary penetration. On the other hand, higher deposition rate may significantly alter the bead height and width values.

Again, at constant WFS, bead height increases with decrease in arc voltage and changes slightly (increases slightly) with increase in CTWD (Fig. 4a). However, bead width and penetration shows opposite behaviour with V and CTWD at particular WFS (Fig. 4b, c). Both the response increases with increase in arc voltage and decreases with decrease in CTWD. Arc voltage maintains the stability of the arc dome and also determines the arc width. Higher arc voltage increases the arc width which ultimately results in bead width enhancement. Similarly bead width will be reduced and consequently bead height increases as the arc voltage decreases. Arc voltage also has a noteworthy effect on controlling the arc force/pressure which is in turn control the primary penetration. Higher arc pressure at higher arc voltage may able to push the molten metal towards the bottom of the weld pool and increases

Table 4 Weld bead geometry characteristics along with HAZ width, deposition rate and grain size of HAZ and weld metal

Sample no.	H (mm)	W (mm)	H/W	P (mm)	A_R (mm ²)	Toe angle (deg)	W_{HAZ} (mm)	D_R (Kg/h)	d_{HAZ} (μm)	d_{WM} (μm)
N1	2.92	8.33	0.350	1.9	16.99	60	1.24	1.989	16.49	13.55
N2	3.94	8.57	0.459	2.75	31.38	60.05	1.47	3.666	18.19	14.74
N3	2.61	8.68	0.300	2.03	16.63	58.5	1.27	1.937	17.7	14.8
N4	3.36	10.82	0.310	3.09	26.78	57	1.77	3.133	20.21	16.41
N5	3.08	8.05	0.382	1.3	17.18	61.5	1.44	2.002	16.13	13.36
N6	5.37	7.41	0.724	1.21	32.62	73	0.95	3.809	16.82	14.59
N7	2.02	8.31	0.243	1.71	16.47	53.5	1.45	1.924	17.52	14.93
N8	2.39	9.13	0.262	2.39	27.01	58	1.81	3.159	19.02	16.03

H bead height, W bead width, H/W convexity index, P depth of penetration, A_R reinforcement area, W_{HAZ} width of HAZ, D_R deposition rate, d_{HAZ} grain size of HAZ, d_{WM} grain size of weld metal

Fig. 3 Macrograph (cross-section) of weld bead geometries under different welding conditions

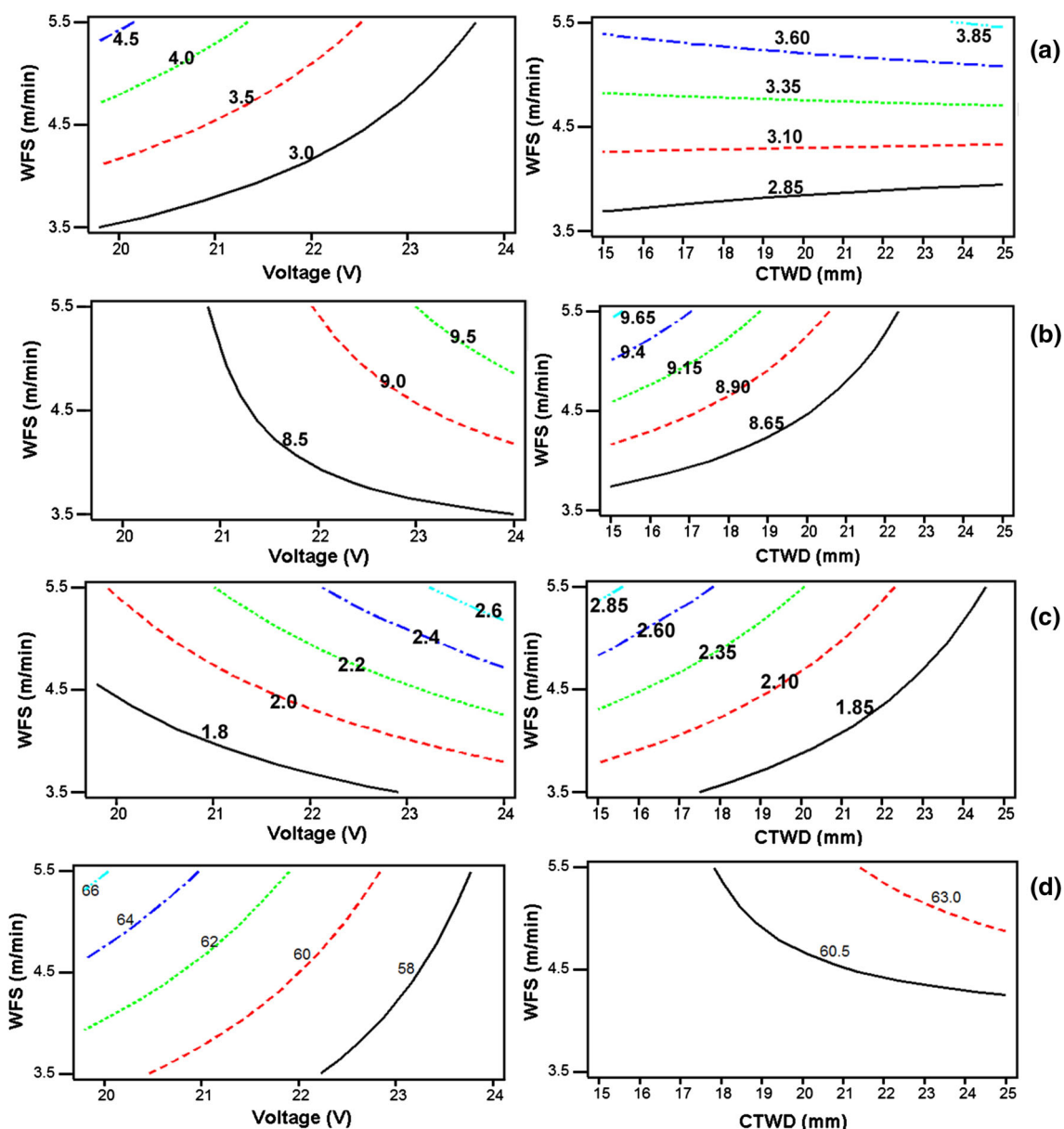
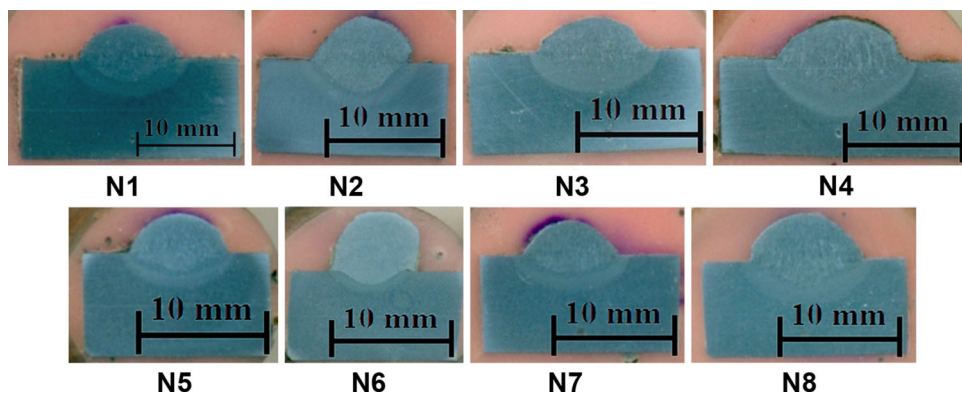


Fig. 4 Contour plot shows the effect of wire feed speed (WFS), arc voltage (V) and contact tip to work-piece distance (CTWD) on **a** bead height, **b** bead width, **c** depth of penetration and **d** toe angle

the primary penetration zone up to a certain extent. On the other hand, CTWD has reverse effect on the bead geometry compare to other parameters. This is due to the fact that higher CTWD reduces the arc pressure and increases the reinforcement height which in turn decreases bead width and penetration. Again, the variations in toe angle with respect to three process parameters are shown in Fig. 4d. At constant CTWD toe angle increases with increase in WFS and decrease in arc voltage. When the arc voltage remain constant toe angle increases with increase in CTWD. Comparing with Fig. 4a, b and d, toe angle of weld deposit increases with increase in bead height and undoubtedly decreases with increase in bead width. The effect of bead height and width can be better understood by considering convexity index (H/W). It is observed that higher toe angles are mainly situated with higher convexity index (H/W) values as shown in Table 4.

3.2 Multiple Linear Regression Models for Bead Geometry

In the regression analysis, the convexity index (H/W) has been considered as a prime response instead of considering individual responses (i.e. bead height and bead width). Here it is assumed that the convexity index could provide better understanding for the individual responses and their cumulative effect on the bead reinforcement. Apart from this, other responses such as depth of penetration (P) and reinforcement area (A_R) for bead geometry were individually analysed. We also consider the deposition rate (D_R) as a response due to the fact that it has direct effect on determining the bead geometry. Therefore, welding parameters along with the interactive variables were considered during the regression analysis. From the obtained data for the bead geometry and process parameters (Tables 3 and 4), the multiple linear regression equations were determined and are given below:

$$H/W = 0.510 + 0.287 \times WFS - 0.0201 \times CTWD + 0.0246 \times V - 2.21 \times HI \quad (1)$$

$$S = 0.04385 \quad R - Sq = 96.6\% \quad R - Sq(adj) = 92.1\%$$

$$P \text{ (mm)} = 2.62 + 0.487 \times WFS - 0.0651 \times CTWD - 0.0163 \times V - 2.91 \times H/W \quad (2)$$

$$S = 0.1376 \quad R - Sq = 98.2\% \quad R - Sq(adj) = 95.7\%$$

$$A_R \text{ (mm}^2\text{)} = -2.88 + 5.66 \times WFS - 0.0145 \times CTWD - 0.151 \times V + 10.9 \times H/W \quad (3)$$

$$S = 1.197 \quad R - Sq = 98.8\% \quad R - Sq(adj) = 97.1\%$$

$$D_R \text{ (Kg/h)} = -1.34 + 0.475 \times WFS + 0.0236 \times CTWD - 0.0120 \times V + 2.39 \times H/W + 0.389 \times P \quad (4)$$

$$S = 0.1562 \quad R - Sq = 99.0\% \quad R - Sq(adj) = 96.4\%$$

A result of ANOVA for the regression models of the bead geometry is shown in Tables 5, 6, 7, 8. By comparing with the calculated and the statistical F-ratios, it was seen that the regression models were quite adequate. Also the P-values of these models clearly point out the acceptability of the regression equations. All the adjusted R^2 values are more than 95 % which is again a clear indication of the adequacy of the developed models. The values of weld bead geometry and deposition rate obtained from experiments and those predicted from regression model are plotted in Fig. 5a–d. From the graph, it can be observed that the predicted responses are very close and sometime superimposed on the actual responses which clearly indicate the adequacy of the regression models.

3.3 Evaluation of Microstructure

From optical micrographs as shown in Fig. 6, it is observed that all the weld metals consist of different forms of ferrite morphologies such as grain boundary ferrite (GBF), acicular ferrite (AF), ferrite side plates aligned [FS(A)] etc. This microstructure of weld metals is probably due to the complex interactions between weld thermal cycle, chemical composition, cooling rate, size distribution of non metallic inclusions and the prior austenite grain size. In the present study it is assumed that the weld metal composition remain almost constant due the use of same base metal, filler metal and shielding gas conditions for all the experiments. Therefore the variation in microstructure is solely related with the change in cooling rate or heat input. A closer inspection of the micrographs in Fig. 6 reveals a considerable difference in the weld metal transformation behavior between the high- and the low heat input welds at fixed CTWD (Table 3). The low heat input welds at CTWD of 15 mm shows (Fig. 6a, c) three phase microstructure i.e. the formation of fine GBF along with ferrite with aligned second phase and few AF colonies. For the high heat input welds (Fig. 6b, d), the microstructure is predominantly consist of acicular ferrite and coarse GBF. A similar pattern was observed for the welds within high CTWD (25 mm), although the coarsening of GBF was considerably lower (Fig. 6e–h) compare to their counterparts at lower CTWD. Examining a schematic temperature log-time diagram (Fig. 7) [16], it becomes evident that a faster cooling rate (low heat input) can pass into a fairly

Table 5 ANOVA table for linear regression analysis of Convexity index (H/W)

Source	Degree of freedom	Sum of squares	Mean square	F ratio	P value
Regression model	4	0.164114	0.041028	21.33	0.015
Error	3	0.005770	0.001923		
Total	7	0.169884			

Table 6 ANOVA table for linear regression analysis of Depth of penetration (P, mm)

Source	Degree of freedom	Sum of squares	Mean square	F ratio	P value
Regression model	4	3.03699	0.75925	40.13	0.006
Error	3	0.05676	0.01892		
Total	7	3.09375			

Table 7 ANOVA table for linear regression analysis of Reinforcement area (A_R , mm²)

Source	Degree of freedom	Sum of squares	Mean square	F ratio	P value
Regression model	3	341.91	85.48	59.70	0.003
Error	4	4.29	1.43		
Total	7	346.20			

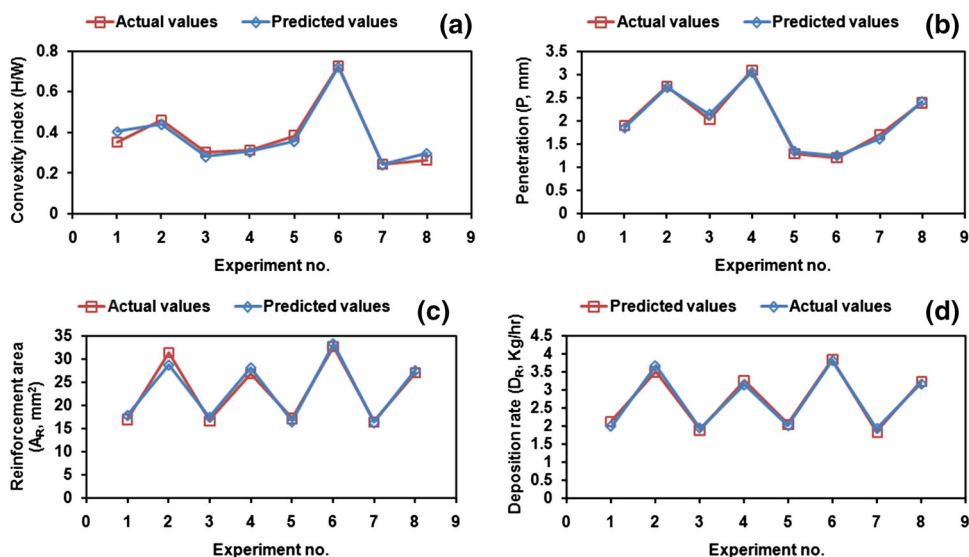
Table 8 ANOVA table for linear regression analysis of Deposition rate (D_R , Kg/h)

Source	Degree of freedom	Sum of squares	Mean square	F ratio	P value
Regression model	5	4.68942	0.93788	38.43	0.026
Error	2	0.04881	0.02441		
Total	7	4.73823			

narrow window of acicular ferrite and aligned ferrite. Whereas, slow cooling rate or high heat input will produce blocky ferrite or grain boundary ferrite and acicular ferrite in expense of FS(A) (Fig. 7). Higher heat input also allows more time for diffusion along the grain boundary and the GBF became coarser. On the other hand, higher CTWD reduces the overall arc current (when other parameters are kept constant) which ultimately reduces the heat input and shifts the cooling curve towards AF region. Therefore, higher CTWD associated with the faster cooling in general produces more AF and finer GBF in final microstructure of weld metals.

The typical heat affected zone (HAZ) microstructures of different bead-on-welds as shown in Fig. 8 reveal different forms of ferrite. The HAZ adjacent to the fusion line represents base metal heated above the A_3 temperature (i.e. 910 °C) during the weld thermal cycle. Significant γ grain growth takes place in the HAZ and large γ grains form due to the partial phase transformation from ferrite to austenite [17]. It should be noted that the actual completion temperature of $\alpha \rightarrow \gamma$ transformation depends on the local heating rate, and varies between different locations in the HAZ. However, using a constant temperature for representing the start of γ grain growth is reasonable, since the grain growth is a thermally activated process and the majority of growth takes place at elevated temperatures [18, 19]. The subsequent phase transformation ($\gamma \rightarrow \alpha$) depends on the cooling rate (applied heat input) of respective bead-on-welds. Faster cooling will produce different types of ferrite morphologies such as primary ferrite, polygonal ferrite, allotriomorphic ferrite, ferrite side plates and few acicular ferrite as shown in Fig. 8a, c, e–g. However, at higher heat input condition significant growth of primary ferrite, polygonal ferrite, and ferrite side plates have been observed in the HAZ microstructure

Fig. 5 Comparison between actual and predicted values of a H/W, b P, c A_R and d D_R



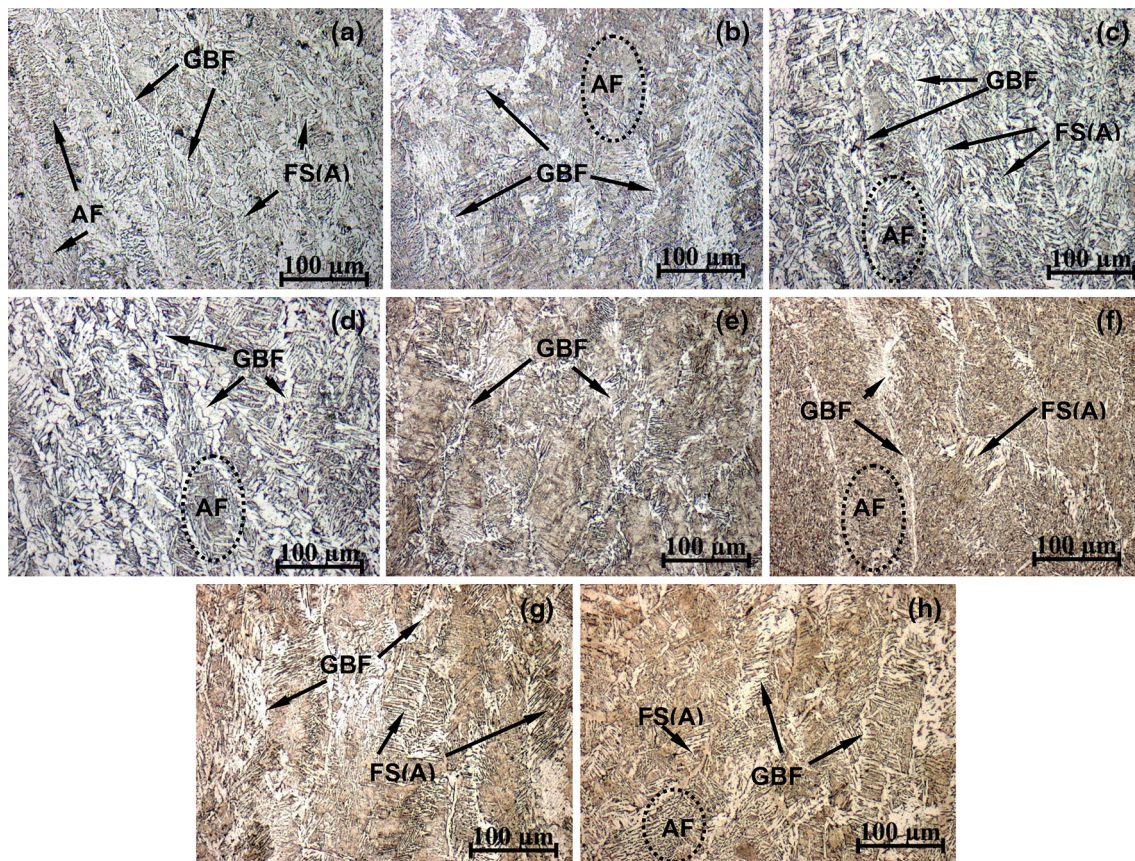


Fig. 6 Microstructure of weld metals **a** N1, **b** N2, **c** N3, **d** N4, **e** N5, **f** N6, **g** N7, and **h** N8

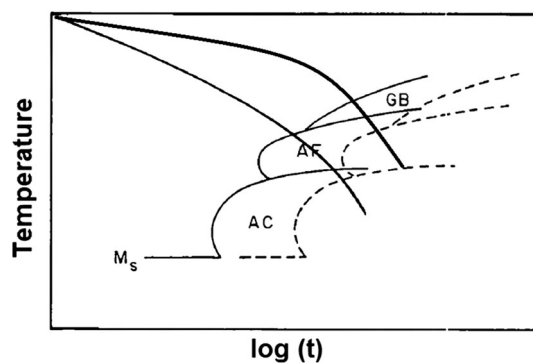


Fig. 7 Simulated temperature log-time CCT diagram that illustrates the variation in microstructure on cooling [16]

(Fig. 8b, d, h). Again, HAZ width (W_{HAZ}) of all bead-on-welds has been measured using AutoCAD 2010 software and presented in Table 4. W_{HAZ} increases with the increase in WFS at fixed arc voltage and CTWD (Table 3). In other word, high heat input in general increases the HAZ width which is obvious because at high heat input more amount of heat has been extracted along the transverse direction of moving heat source.

The average grain size of weld metal and HAZ were calculated using linear intercept method (as per ASTM

E1382) from micrographs of bead-on-welds and the values are presented in Table 4. The grain size of weld metals can be typically correlated with the heat input or the cumulative effect of weld parameters. It is observed from Tables 3 and 4 that the substantial grain growth has been occurred as the heat input increases. Even the variable grain size of HAZ is also the result of different heat input condition. HAZ grains became coarser with the increases in heat input. Therefore, it can be stated that width of HAZ and grain size of bead-on-welds are significantly affected by the cumulative effect of input variables. Hence, in the next section an attempt has been made to develop models to predict grain size and HAZ width from different variables.

3.4 Multiple Linear Regression Models for HAZ Width and Grain Size

In the regression analysis width of HAZ (W_{HAZ}), grain size of weld metal (d_{WM}) and HAZ (d_{HAZ}) have been considered as responses. To determine the regression model for W_{HAZ} five input variables such as WFS, CTWD, V, P and A_R have been considered. Among these variables first three are the primary process variables and later two are the interactive variables as given in Eqs. (2) and (3). Similarly,

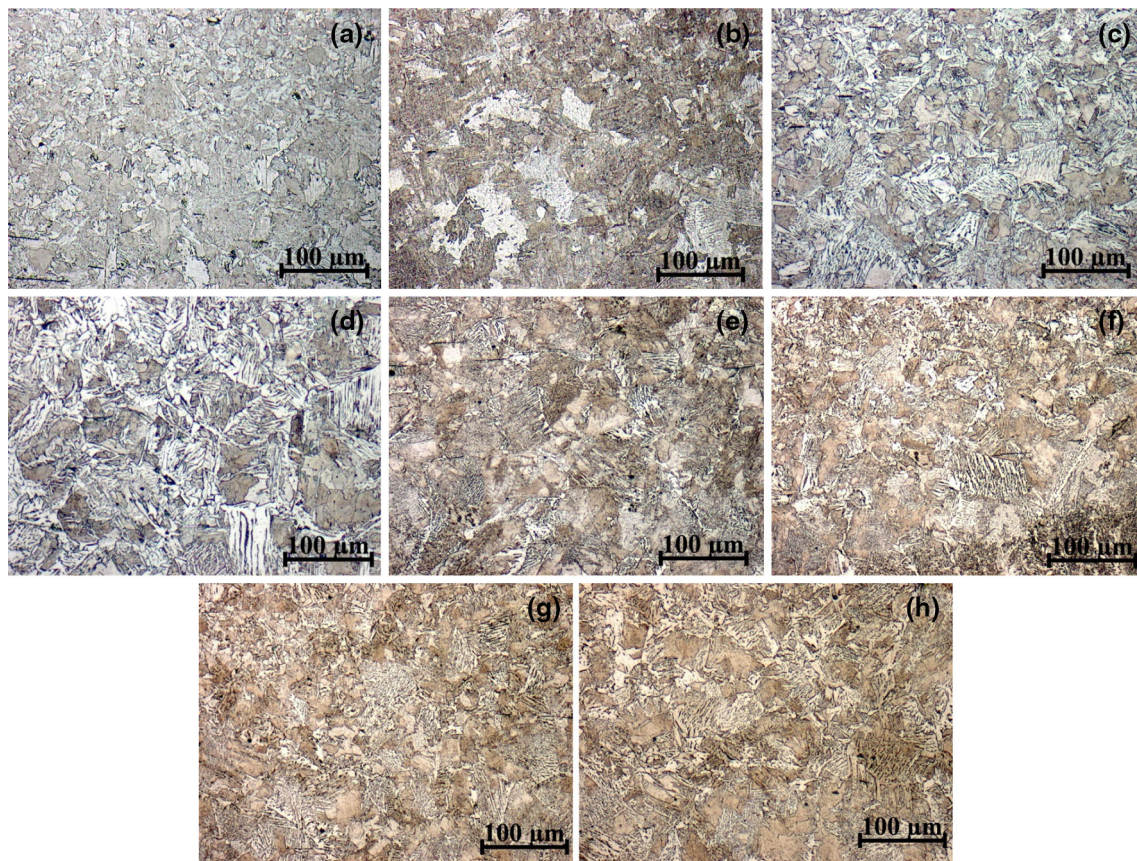


Fig. 8 Microstructure of heat affected zone (HAZ) **a** N1, **b** N2, **c** N3, **d** N4, **e** N5, **f** N6, **g** N7, and **h** N8

for d_{WM} and d_{HAZ} primary process parameters and interactive variables (such as HI) were used. Interactive variables are used in these models due to the fact that these variables can provide necessary cumulative effect of the several parameters. From the obtained data for the bead geometry and process parameters (Tables 3 and 4), the multiple linear regression equations were determined and are given below:

$$W_{HAZ}(mm) = 1.11 - 0.012 \times WFS + 0.0472 \times CTWD - 0.104 \times V + 4.24 \times HI - 0.0552 \times A_R \tag{5}$$

$S = 0.02827$ $R - Sq = 99.7\%$ $R - Sq(adj) = 99.0\%$

$$d_{WM}(\mu m) = 4.65 + 0.571 \times WFS - 0.0070 \times CTWD + 0.331 \times V + 0.69 \times HI \tag{6}$$

$S = 0.1550$ $R - Sq = 99.1\%$ $R - Sq(adj) = 97.8\%$

$$d_{HAZ}(\mu m) = 8.67 + 0.037 \times WFS + 0.0059 \times CTWD + 0.163 \times V + 7.43 \times HI \tag{7}$$

$S = 0.3077$ $R - Sq = 97.8\%$ $R - Sq(adj) = 95.2\%$

A result of ANOVA for the regression models of the W_{HAZ} , d_{WM} and d_{HAZ} is shown in Tables 9, 10, 11 respectively. By comparing with the calculated and the statistical F-ratios, it was seen that the regression models were quite adequate. Also the P values of these models clearly point out the acceptability of the regression equations. All the adjusted R^2 values are more than 93 % which is again a clear indication of the adequacy of the developed models. The values of W_{HAZ} , d_{WM} and d_{HAZ} obtained from experiments and those predicted from regression model are plotted in Figs. 9a-c. From the graph, it can be observed that the predicted responses are very close and sometime superimposed on the actual responses which clearly indicate the adequacy of the regression models.

Table 9 ANOVA table for linear regression analysis of Width of HAZ (W_{HAZ} , mm)

Source	Degree of freedom	Sum of squares	Mean square	F ratio	P value
Regression model	5	0.55240	0.11048	138.23	0.007
Error	2	0.00160	0.00080		
Total	7	0.55400			

Table 10 ANOVA table for linear regression analysis of Grain size of weld metal (d_{WM} , μm)

Source	Degree of freedom	Sum of squares	Mean square	F ratio	P value
Regression model	4	7.7336	1.9334	80.48	0.002
Error	3	0.0721	0.0240		
Total	7	7.8057			

Table 11 ANOVA table for linear regression analysis of Grain size of HAZ (d_{HAZ} , μm)

Source	Degree of freedom	Sum of squares	Mean square	F ratio	P value
Regression model	4	12.7056	3.1764	33.56	0.008
Error	3	0.2840	0.0947		
Total	7	12.9896			

4 Conclusion

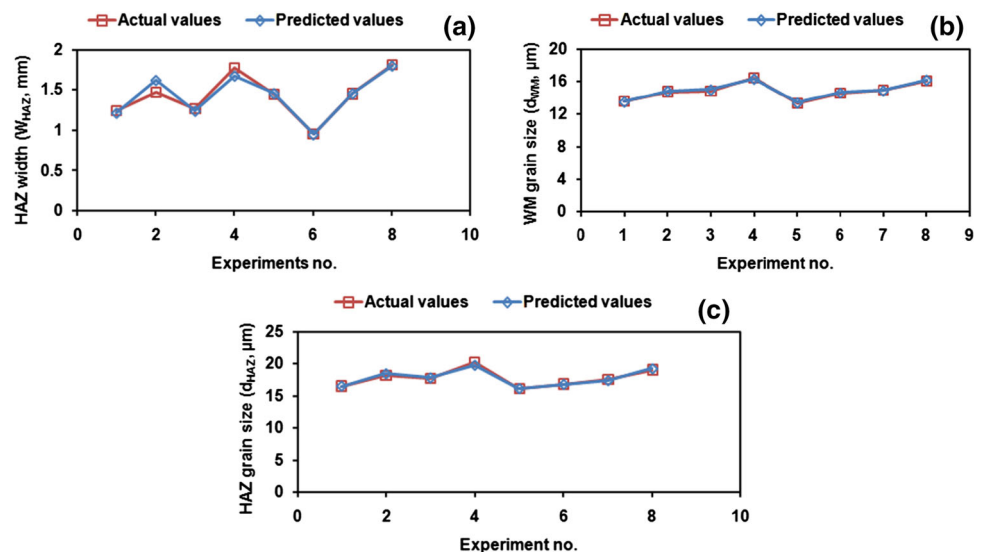
The following conclusions can be drawn from the present study:

- Convexity index (H/W) is mainly affected by the heat input and wire feed speed. High negative coefficient of

heat input impart a dissent effect on the H/W (i.e. increase in HI reduces H/W) and positive coefficient of wire feed speed puts a positive impact on H/W. It is likely to be mentioned here that, toe angle of weld deposit increases with increase in bead height and undoubtedly decreases with increase in bead width.

- Depth of penetration (P) and reinforcement area (A_R) are significantly affected by wire feed speed and convexity index. It is evident from contour plots that the increase in wire feed speed considerably increases the depth of penetration. Again, deposition rate (D_R) is also adequately expressed as a function of several variables and mostly affected by wire feed speed and convexity index.
- In the present study width of HAZ (W_{HAZ}) is expressed as a function of wire feed speed, contact-tip-to-work-piece distance, voltage, reinforcement area and heat input. Among these variables contact-tip-to-work-piece distance and heat input have positive impact and other three variables have diminishing effect on the W_{HAZ} .
- In general, it can be stated that the grain size of weld metal and HAZ is mainly affected by the heat input and increases with the increase in heat input. It is likely to be mentioned here that, the low heat input shows three phase microstructure i.e. the formation of fine GBF along with ferrite with aligned second phase and few AF colonies. For the high heat input the microstructure predominantly consists of AF and coarse GBF.
- The empirical equations developed by multiple linear regression analysis were able to give adequate insight on the correlations between variables and entirely valid for the range of parameters (such as current: 120–195 A; voltage: 19.5–24 V; wire feed speed: 3.5–5.5 m/min; contact-tip-to-work-piece distance: 15–25 mm) and material used in the present study.

Fig. 9 Comparison between actual and predicted values of **a** W_{HAZ} , **b** d_{WM} and **c** d_{HAZ}



Acknowledgments The authors would like to thank all the Research scholars of Welding Technology Centre, Metallurgical and Material Engineering Department, Jadavpur University and also to Dr. Dipak Kumar Mondal, H.O.D. Mechanical Engineering Department, college of Engineering & Management, Kolaghat; for their valuable support.

References

1. Ganjigatti J P, Pratihar D K, and Roy Choudhury A, *J Mater Process Technol* **189** (2007) 352.
2. Shmoda T, and Doherty J, *The Welding Institute Report* **74** (1978).
3. Chandel R S, Seow H P, and Cheong F L, *J Mater Process Technol* **72** (1997) 124.
4. Jou M, *J Manuf Sci Eng* **125** (4) (2003) 801.
5. Gunaraj V, and Murugan N, *J Mater Process Technol* **95** (1999) 246.
6. Gunaraj V, and Murugan N, *Weld J* **10** (2000) 286s.
7. Gunaraj V, and Murugan N, *Weld J* **11** (2000) 331s.
8. Kim I S, Jeong Y J, Sona I J, Kim I J, Kimb J Y, Kim I K, and Yarlagadda P K D V, *J Mater Process Technol* **140** (2003) 676.
9. Kim I S, Son K J, Yang Y S, and Yarlagadda P K D V, *Int J Mach Tools Manuf* **43** (2003) 763.
10. Kim I S, Son J S, Kim I G, Kim J Y, and Kim O S, *J Mater Process Technol* **136** (2003) 139.
11. Lee J I, and Rhee S, Prediction of process parameters for gas metal arc welding by multiple regression analysis, in *Proceedings of the Institution of Mechanical Engineers. Part B*, **214** (2000) p 443.
12. Ganjigatti J P, Pratihar D K, and Roy Choudhury A, *J Mater Process Technol* **189** (2007) 352.
13. Gunaraj V, and Murugan N, *Weld J* **1** (2002) 94s.
14. Yang L J, Chandel R S, and Bibby M J, *Weld J* **1** (1993) 11s.
15. Rao P S, Gupta O P, Murty S S N, and Koteswara Rao A B, *Int J Adv Manuf Technol* **45** (2009) 496.
16. Francis R E, Jones J E and Olson D L, *Weld J* **11** (1990) 408s.
17. Zhang W, Elmer J W and DebRoy T, *Sci Technol Weld Join* **10** (2005) 574.
18. Yang Z, Sista S, Elmer J W and Debroy T, *Acta Mater* **48** (2000) 4813.
19. Mishra S and Debroy T, *Acta Mater* **52** (2004) 1183.